

Mbd2 deficiency alleviates retinal cell apoptosis via the miR-345-5p/Atf1 axis in high glucose injury and streptozotocin-induced diabetic mice

Yanni Ge,^{1,2,3} Ran Zhang,^{1,2,3} Yuqing Feng,^{1,2} Jinfang Lu,^{1,2} and Huiling Li^{1,2}

¹Department of Ophthalmology, The Second Xiangya Hospital, Central South University, Changsha, Hunan 410011, China; ²Hunan Clinical Research Center of Ophthalmic Disease, Changsha, Hunan 410011, China

DNA methylation is considered to play an important role in the development of diabetic retinopathy. Here, our goal was to investigate the precise role of methyl-CpG binding domain protein 2 (Mbd2) in the apoptosis of retinal ganglion cells (RGCs) in the early diabetic retina. Mbd2 was significantly upregulated after high glucose (HG) treatment and played a proapoptotic role in RGCs during HG-induced apoptosis. Combining ChIP and gene microarray datasets, the results showed that Mbd2 possessed potential binding sites for miR-345-5p, thereby elevating the expression levels of miR-345-5p via the enhancement of promoter demethylation. Activating transcription factor 1 (Atf1) played an anti-apoptotic role during the process of apoptosis in RGCs and acted as the target gene for miR-345-5p. Furthermore, the number of surviving RGCs in the diabetic retina was increased in Mbd2-knockout mice when compared with wild-type mice and the visual function became better accordingly. Collectively, our data demonstrated that the HG-induced overexpression of Mbd2 in the retina was partly responsible for the apoptosis of retinal neuronal cells through the miR-345-5p/Atf1 axis. Therefore, the targeting of Mbd2 might represent a novel therapeutic strategy for the treatment of neurodegeneration in the early diabetic retina.

INTRODUCTION

Diabetic retinopathy (DR) remains a leading cause of blindness in the working-age population.¹ At present, retinopathy is characterized clinically by demonstrable vascular abnormalities; moreover, microvascular complications can trigger irreversible retinal damage. The treatments available at present focus mostly on vascular complications of the disease in the advanced stages. Nevertheless, reductions in the thickness of the retinal ganglion cell (RGC) layer have been confirmed in the earliest stages of DR.²⁻⁴ Available evidence strongly indicates that neuronal cells in the retina are also affected by diabetes. Earlier research also reported the loss of surviving RGCs after 1 month of streptozotocin (STZ)-induced diabetes in a rat model.⁵ A more recent study reported obvious inner retinal thinning and ganglion cell loss in experimental mouse models of diabetes but without any effect on capillaries or pericyte density.⁶ In particular, studies involving human donors with diabetes demonstrated that vascular damage in the human retina was preceded by an increase in neural apoptosis.⁷ Other clinical evidence

showed that the early neurodegenerative effects on RGCs occurred prior to the clinical signs of microvasculopathy in patients with diabetes.⁶ Therefore, we hypothesized that neural cell death in the retina is an early event in diabetes and may possibly affect the onset and progression of disease. However, little is known about the precise mechanisms that underlie the process of apoptosis in RGCs in the diabetic retina.

DNA methylation is considered to represent a vital mechanism involved in epigenetic modification and plays an essential role in the regulation of gene expression in many disease conditions,⁸ including DR.^{9,10} Previous research has also demonstrated that DNA methylation is involved in retinal cell death.¹¹ Methyl-CpG binding domain protein 2 (Mbd2) is considered to act as a reader of DNA methylation.¹² Previous studies have reported that Mbd2 plays a key role in the apoptosis of renal and endothelial cells when induced by vancomycin and ischemic injury, respectively.^{13,14} More recently, our own group demonstrated for the first time that Mbd2 mediates the apoptosis of RGCs when induced by ischemic injury and acts via the regulatory action of long non-coding RNAs (lncRNAs).¹⁵ However, it was not clear whether Mbd2 was involved in the apoptosis of RGCs induced under high glucose (HG) conditions. In addition, there is an abundance of evidence to indicate that cellular microRNAs (miRNAs) are involved in a range of cellular processes¹⁶ and could act as mediators in the regulation of pathways associated with cell growth and apoptosis,¹⁷ and may even mediate the apoptosis of neuronal cells in the retina.^{18,19} Interestingly, several studies have demonstrated that Mbd2 might directly regulate miRNAs to mediate apoptosis in renal and tumor cells. More recently, two studies revealed that the inhibition of miR-100 or miR-134 could protect against H₂O₂-induced apoptosis in RGCs.^{20,21}

According to these earlier findings, we hypothesized that Mbd2 mediates HG-induced apoptosis in RGCs by regulating the action of

Received 30 December 2020; accepted 29 October 2021;
<https://doi.org/10.1016/j.omtn.2021.10.026>.

³These authors contributed equally

Correspondence: Huiling Li, MD, Department of Ophthalmology, The Second Xiangya Hospital, Central South University, Changsha, Hunan 410011, China.

E-mail: lihuiling@csu.edu.cn



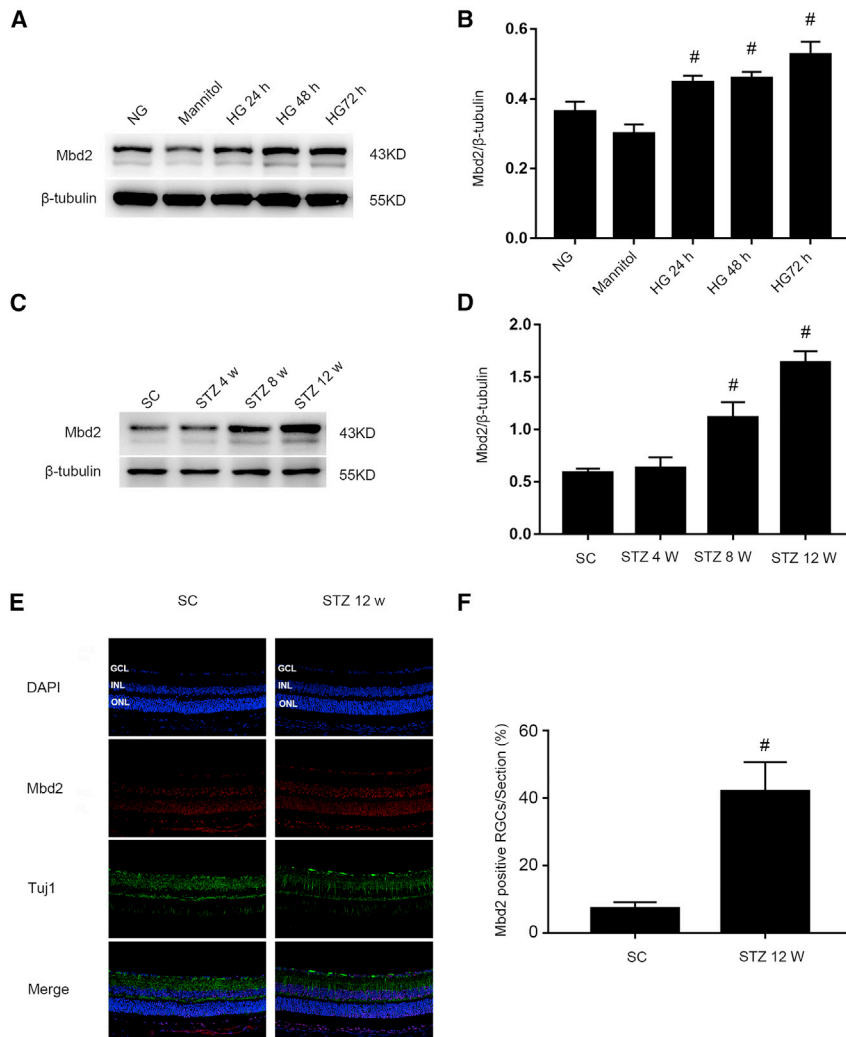


Figure 1. The expression of Mbd2 in RGCs following exposure to HG conditions and in the retina of STZ-induced diabetic mice

Representative images of western blotting and the quantification of Mbd2 expression in mice RGCs (A and B) and in diabetic retina (C and D) at different time points. Representative images of retina sections (E) and the quantification of Mbd2 in diabetic retina (F). Immunofluorescent staining of Mbd2 (red) showed in the RGC layer. The proportion (%) of Mbd2-positive cells were counted in four different fields from three different sections in each retina and then normalized by DAPI staining cells in the ganglion cell layer.

GCL, ganglion cell layer; INL, inner nuclear layer; ONL, outer nuclear layer. Scale bar, 20 μ m. Data are given as mean \pm SD of five independent experiments; #p < 0.05 versus NG or SC.

72 h than those in a normal glucose group *in vitro* (Figures 1A and 1B). We also investigated the levels of Mbd2 protein in the retinas of diabetic mice at 4 weeks, 8 weeks, and 12 weeks after STZ injection. When compared with the sodium citrate (SC)-injected group, the expression levels of Mbd2 significantly began to rise from 8 weeks to 12 weeks after the injection of STZ (Figures 1C and 1D). Immunofluorescence staining further confirmed the increased expression of Mbd2 in diabetic retina, particularly in the ganglion cell layer; Mbd2 was located in the nucleus of the RGCs (Figures 1E and 1F).

The downregulation of Mbd2 protected RGCs from HG-induced apoptosis

To investigate the role of Mbd2 in the diabetic retina, we applied Mbd2 siRNA to suppress the expression of Mbd2. HG interference induced apoptosis in RGCs and increased the expression of levels of cleaved caspase3. The increased rate of apoptosis induced by HG conditions was reduced following the suppression of Mbd2 (Figures 2A and 2B); similarly, the levels of cleaved caspase3 were also reduced (Figures 2C–2F). We also constructed an Mbd2 plasmid; the overexpression of Mbd2 aggravated the apoptotic process in RGCs (Figures 2G and 2H); the expression of cleaved caspase3 also increased (Figures 2I–2L). Our data suggested that Mbd2 acts as a pro-apoptosis factor in the HG-induced apoptosis of RGCs.

Mbd2 promoted the demethylation of miR-345-5p at the promoter region

To gain further insight into the molecular mechanisms underlying the Mbd2-mediated induction of apoptosis in RGCs under high HG conditions, and to determine whether Mbd2 regulates the expression of miRNA, we conducted gene microarray analysis to detect differentially expressed miRNAs (Figure 3A). Based on expression data, we focused

miRNAs. Our analysis showed that Mbd2 may possess potential binding sites for miR-345-5p and that these sites can increase expression levels. We also demonstrated that activating transcription factor 1 (Atf1), the target gene for miR-345-5p, plays an anti-apoptotic role during the apoptosis of RGCs. Furthermore, *in vivo* studies showed that the knockout of Mbd2 in a mouse model ameliorated the apoptosis of RGCs induced by diabetes. Collectively, our results demonstrated that the HG-induced overexpression of Mbd2 in the retina is partly responsible for the apoptosis of retinal neuronal cells and acts via the miR-345-5p/Atf1 axis. Thus, targeting Mbd2 may represent a novel therapeutic strategy for the early diabetic retina.

RESULTS

Mbd2 expression was induced in RGCs under HG condition and increased in diabetic retina

To detect the expression levels of Mbd2 in RGCs from mice with DR, RGCs were cultured in HG conditions for 24 h, 48 h, and 72 h. The expression levels of Mbd2 were significantly higher from 24 h to

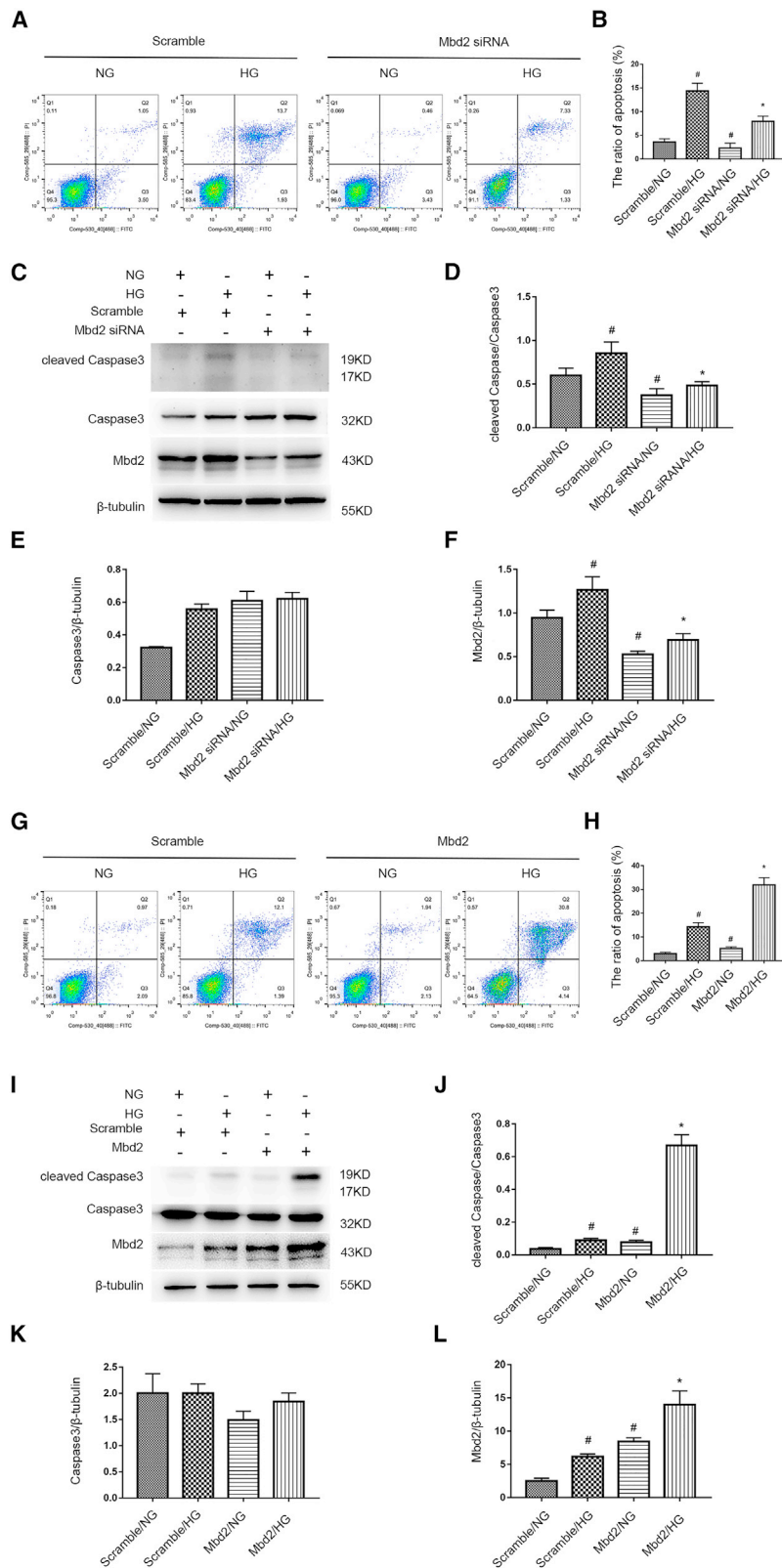
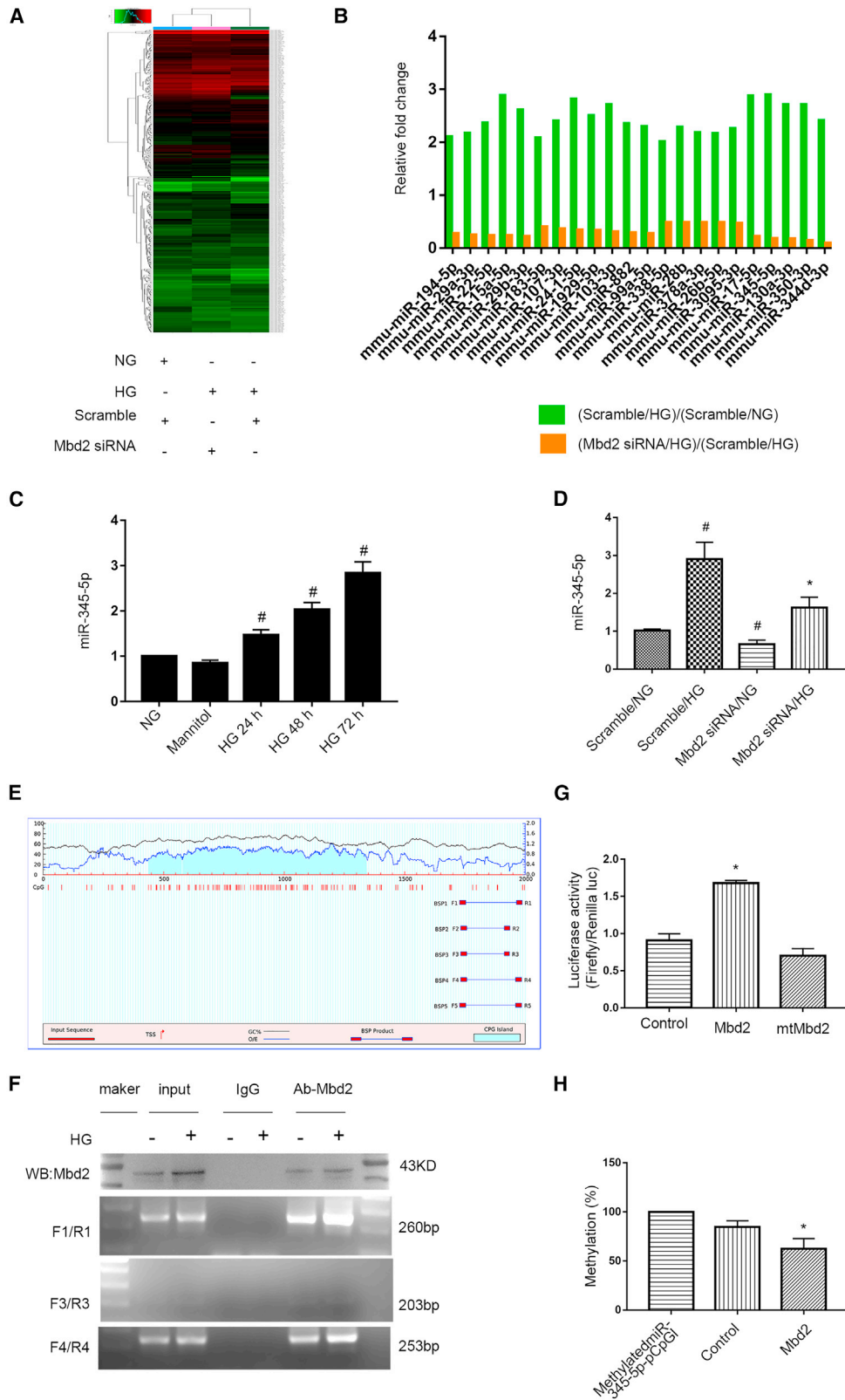


Figure 2. HG-induced apoptosis in RGCs was mediated by Mbd2

Representative images of flow cytometric results (A) and the analysis of apoptosis rate in RGCs (B) in NG, HG, NG + Mbd2 siRNA(50 nM), and HG + Mbd2 siRNA RGCs. Changes in the protein levels of Mbd2 and cleaved caspase3 after the transfection of Mbd2 siRNA, (C) statistical analysis of western blotting results following normalization by β -tubulin and caspase3 (D–F). Representative images of flow cytometric results (G) and the analysis of apoptosis rate in RGCs (H). Changes in the protein level of Mbd2 and cleaved caspase3 after transfection of the Mbd2 plasmid (I) and statistical analysis of western blotting results when normalized by β -tubulin and caspase3 (J–L). Data are shown as the mean \pm SD of five independent experiments; #p < 0.05 versus Scramble/NG; *p < 0.05 versus Scramble/HG.



(legend on next page)

on candidate miRNAs that were upregulated by more than 2-fold in the RGCs after the induction of HG. Figure 3B shows a summary of the 22 most upregulated miRNAs that were confirmed to be downregulated in cells that were treated with Mbd2 siRNA. Of these 22 miRNAs, we found that miR-345-5p was the most highly upregulated (by 2.9-fold) (Figure 3B). Furthermore, our RT-qPCR data confirmed that the expression levels of miR-345-5p were upregulated by HG conditions from 24 h to 72 h (Figure 3C); levels of miR-345-5p were downregulated following the suppression of Mbd2 (Figure 3D). We used MethPrimer 2.0 software to predict potential Mbd2 binding sites (mBS1-5) in the miR-345-5p promoter (Figure 3E). Among the five pairs of primers used, chromatin immunoprecipitation (ChIP) analysis showed that mBS1, mBS3, and mBS4 were all Mbd2 binding sites in the miR-345-5p promoter (Figure 3F). We also cloned the promoter of miR-345-5p (including the methylated CG DNA) into a pCpG1 vector. This vector was then co-transfected with Mbd2 or mtMbd2 (mutational Mbd2; involving the deletion of the DNA methylation domain) plasmids. Luciferase activity was significantly upregulated by co-transfection with the Mbd2 plasmid but not the mtMbd2 plasmid (Figure 3G). Furthermore, the methylation level of the miR-345-5p promoter was also obviously reduced by the administration of exogenous Mbd2 (Figure 3H). These results showed that Mbd2 promotes the demethylation of miR-345-5p at its promoter region, thus resulting in the upregulation of miR-345-5p in RGCs.

The downregulation of miR-345-5p alleviated HG-induced apoptosis in RGCs

MiR-345-5p has been reported to be associated with cholangiocarcinoma²² and prostate cancer^{23,24}; however, its potential role in the apoptosis of RGCs has yet to be reported. Thus, we transfected miR-345-5p inhibitor (anti-miR-345-5p) into RGCs to inhibit the expression of miR-345-5p (Figure 4C). Interestingly, the rate of apoptosis in RGCs was significantly reduced following the suppression of miR-345-5p (Figures 4A and 4B). Furthermore, the expression levels of cleaved caspase3 were reduced by the administration of anti-miR-345-5p (Figures 4D–4F). However, compared with the transfection of miR-345-5p inhibitor (anti-miR-345-5p), the transfection of miR-345-5p mimic presented completely opposite results (Figures 4G–4L). Thus, our data suggest that miR-345-5p promotes apoptosis in RGCs under HG conditions.

Atf1 was a direct target for miR-345-5p

Recent studies have reported that Atf1 plays a role in cell apoptosis via the activation of a subset of apoptosis-related genes,²⁵ and is also a

target gene for miR-30a&c.^{26,27} The MiRbase database (www.mirbase.org) predicts two miR-345-5p binding sites in the 3' UTR of Atf1 mRNA, indicating Atf1 may be a target gene of miR-345-5p (Figure 5A). These binding sites were cloned into the pmirGLO vector. The miR-345-5p mimic markedly suppressed the luciferase activity of the wild-type (WT) Atf1 3' UTR but not the MUT1 or MUT2 constructs (Figure 5B). RT-qPCR analysis demonstrated that anti-miR-345-5p reversed the suppression of Atf1 induced in RGCs by HG (Figure 5C). These RT-qPCR results were further confirmed by immunoblotting (Figures 5D and 5E). Furthermore, HG markedly inhibited the expression levels of Atf1 in RGCs at certain time points (Figures 5F and 5G). To confirm if Atf1 plays an anti-apoptotic role during HG-induced apoptosis in RGCs, we suppressed the expression of Atf1 using siRNA. Flow cytometry (FCM) analysis showed that Atf1 siRNA notably aggravated HG-induced apoptosis in RGCs (Figures 5H and 5I). FCM results were further confirmed by immunoblot analysis of Atf1 and cleaved caspase3 expression (Figures 5J–5M). Collectively, these data suggest that the anti-apoptotic gene Atf1 is a target gene for miR-345-5p and plays a role in the pathogenic process that leads to retinal cell death induced by HG.

The inhibition of Mbd2 alleviated apoptosis in RGCs *in vitro* via the miR-345-5p/Atf1 axis

Next, we observed the effects of an miR-345-5p mimic on apoptosis in RGCs induced by Mbd2 during HG treatment. FCM analysis demonstrated that Mbd2 siRNA markedly attenuated HG-induced apoptosis in RGCs; however, this was reversed by the miR-345-5p mimic (Figures 6A and 6B). The downregulated expression of cleaved caspase3 and the upregulated expression of Atf1 induced by Mbd2 siRNA were also reversed by the overexpression of miR-345-5p (Figures 6C–6H). Therefore, our data indicate that the overexpression of miR-345-5p reduced the Mbd2 siRNA-mediated protection against apoptosis in RGCs.

Diabetes-induced apoptosis in RGCs was ameliorated in Mbd2 knockout mice

Although Mbd2 played a pro-apoptosis role in the HG-induced apoptosis of RGCs *in vitro* via the miR-345-5p/Atf1 pathway, the function of Mbd2 in the diabetic retina *in vivo* had not been elucidated. Thus, we created a model of DR in Mbd2 knockout mice (Mbd2^{-/-}) and compared these with WT littermates (Mbd2^{+/+}) over 5 consecutive days of STZ injection. Twelve weeks after STZ injection, the mice were killed and the retinas collected. The number of surviving RGCs in diabetic Mbd2^{-/-} retina was higher than that in

Figure 3. Mbd2 directly regulated the expression of miR-345-5p

(A) A representative heatmap of gene expression obtained by microarray analysis in NG, HG, and Mbd2 siRNA groups. (B) The 22 most upregulated miRNAs when comparing the HG group with the NG group; meanwhile, the miRNAs were downregulated in Mbd2 siRNA/HG group when compared with the HG group. The expression levels of miR-345-5p after HG interference at the indicated time points (C) (#p < 0.05 versus NG) and after the transfection of Mbd2 siRNA (D) (#p < 0.05 versus Scramble/HG), as confirmed by RT-qPCR. (E) CpG islands within the miR-345-5p promoter were determined and five primer pairs were designed by MethPrimer 2.0 software. (F) ChIP assay detection of potential binding sites between Mbd2 and the promoter of miR-345-5p. (G) The miR-345-5p-promoter-pCpG1 construct was co-transfected with Mbd2 plasmid, mtMbd2 plasmid, or empty vector (control), and each group was transfected with a renilla plasmid (*p < 0.05 versus mtMbd2). (H) The proportion (%) of CpG-DNA methylation in the miR-345-5p promoter was calculated after co-transfection with the Mbd2 plasmid or empty vector (control) (*p < 0.05 versus Control).

Data are shown as the mean ± SD of five independent experiments.

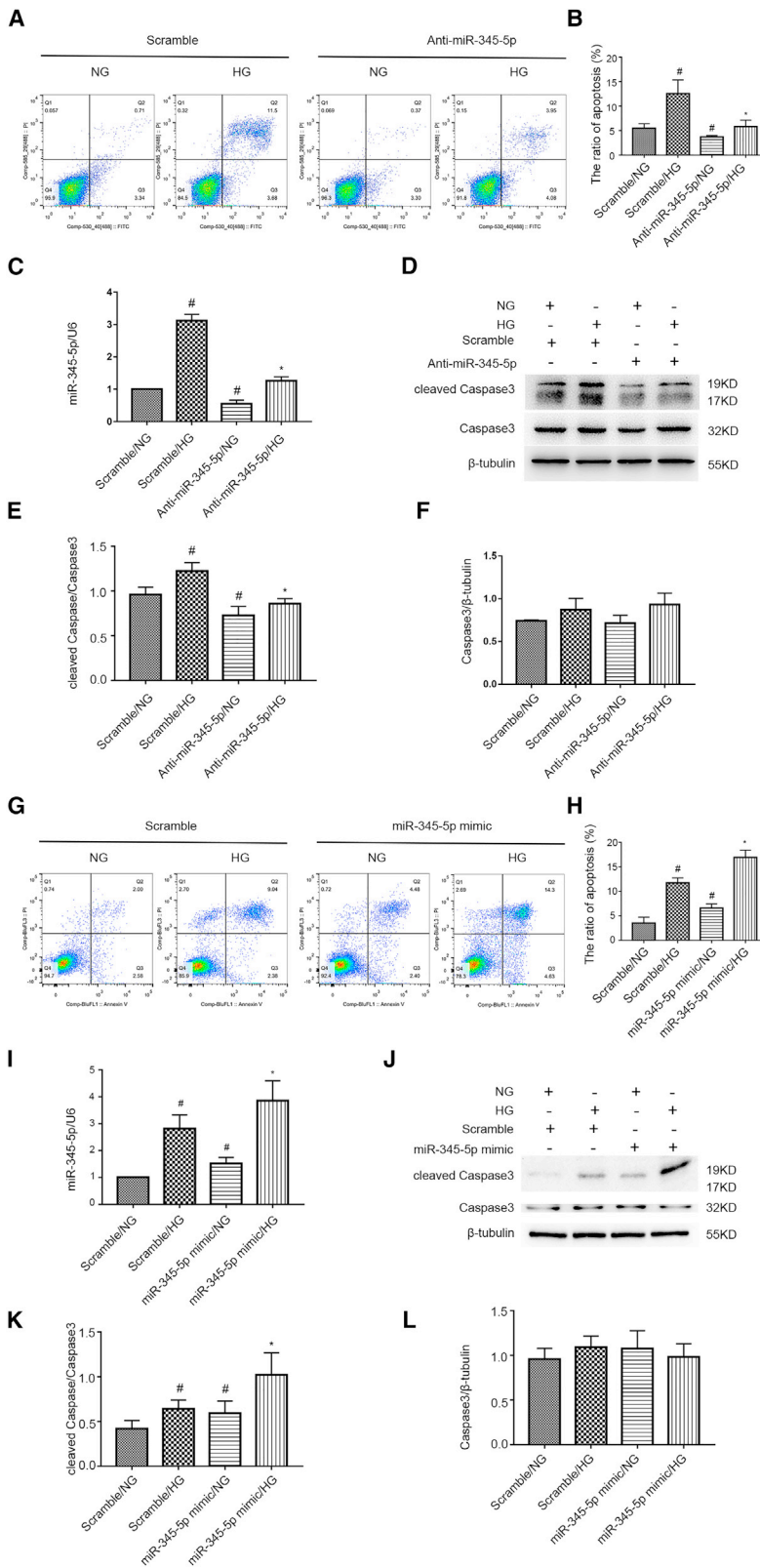


Figure 4. MiR-345-5p mediated HG-induced apoptosis in RGCs

The apoptosis rate of RGCs after HG interference and transfection with anti-miR-345-5p (50 nM), as determined by flow cytometry (A and B). (C) RT-qPCR detected the expression levels of miR-345-5p. Expression changes of cleaved caspase3 after transfection with anti-miR-345-5p (D) and statistical analysis of western blotting as normalized by β -tubulin and caspase3 (E and F). The apoptosis rate of RGCs after HG interference and transfection with miR-345-5p mimic (50 nM), as determined by flow cytometry (G and H). (I) RT-qPCR detected the expression levels of miR-345-5p. Expression changes of cleaved caspase3 after transfection with miR-345-5p mimic (J) and statistical analysis of western blotting as normalized by β -tubulin and caspase3 (K and L). Data are shown as the mean \pm SD of five independent experiments; #p < 0.05 versus Scramble/NG; *p < 0.05 versus Scramble/HG.

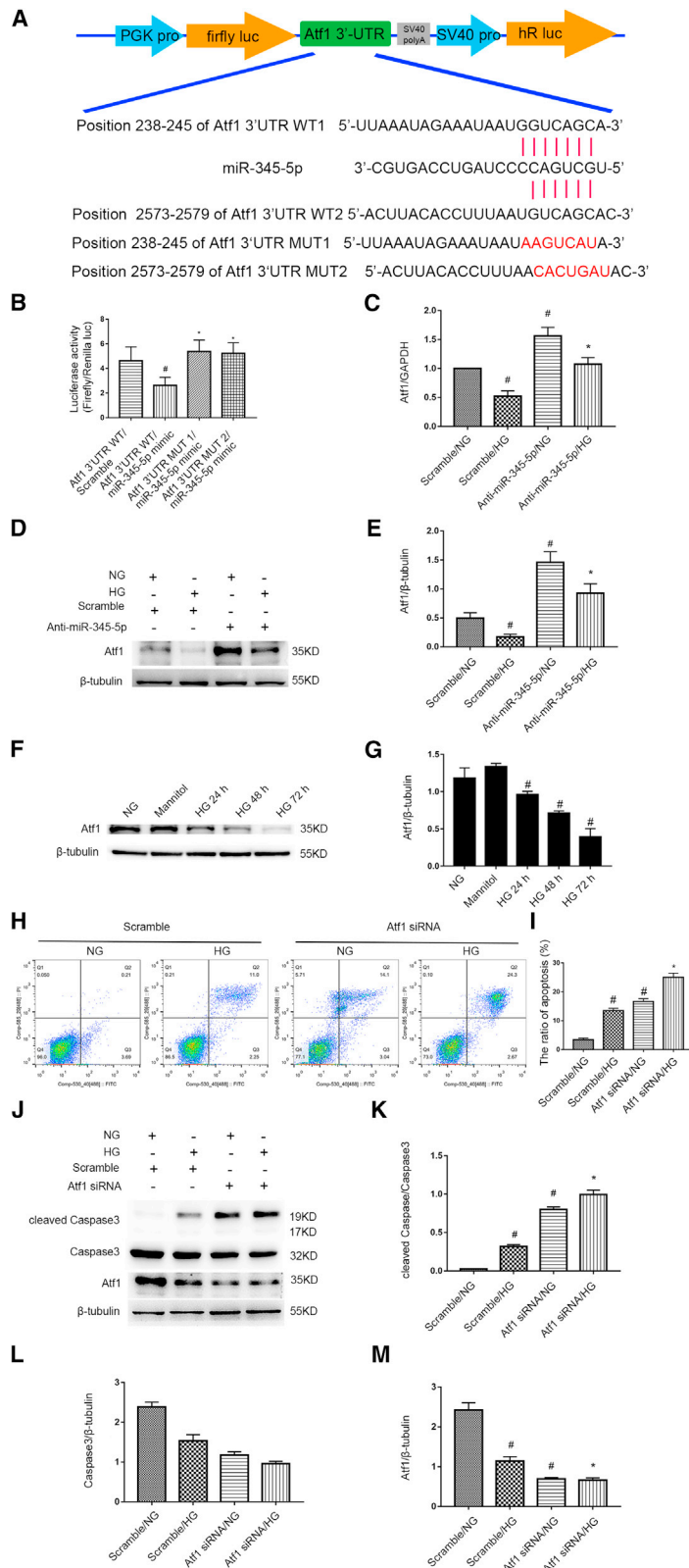


Figure 5. Atf1 is the target gene for miR-345-5p

(A) Atf1 was predicted as the target gene for miR-345-5p by miRbase; there are two complementary binding sites at the 3' UTR region in Atf1. (B) These binding sites were cloned into the pmirGLO vector and luciferase activity was detected after co-transfection with miR-345-5p mimic (#p < 0.05 versus Atf1 3' UTR WT/Scramble; *p < 0.05 versus Atf1 3' UTR WT/miR-345-5p mimic). (C) RT-qPCR showed that the expression levels of Atf1 at mRNA were downregulated in response to the administration of miR-345-5p. (D and E) Western blotting was used to detect the protein levels of Atf1. (F and G) The expression of Atf1 decreased after HG interference at the indicated time point (#p < 0.05 versus NG). RGCs were transfected with 50 nM Atf1 siRNA and followed by 72 h of HG interference. (H and I) The rate of apoptosis was analyzed by flow cytometry. Expression changes in the protein levels of Atf1 and cleaved caspase3 after the transfection of Atf1 siRNA (J), and statistical analysis of western blotting as normalized by β -tubulin and caspase3 (K–M). Data are shown as the mean \pm SD of five independent experiments; #p < 0.05 versus Scramble/NG; *p < 0.05 versus Scramble/HG.

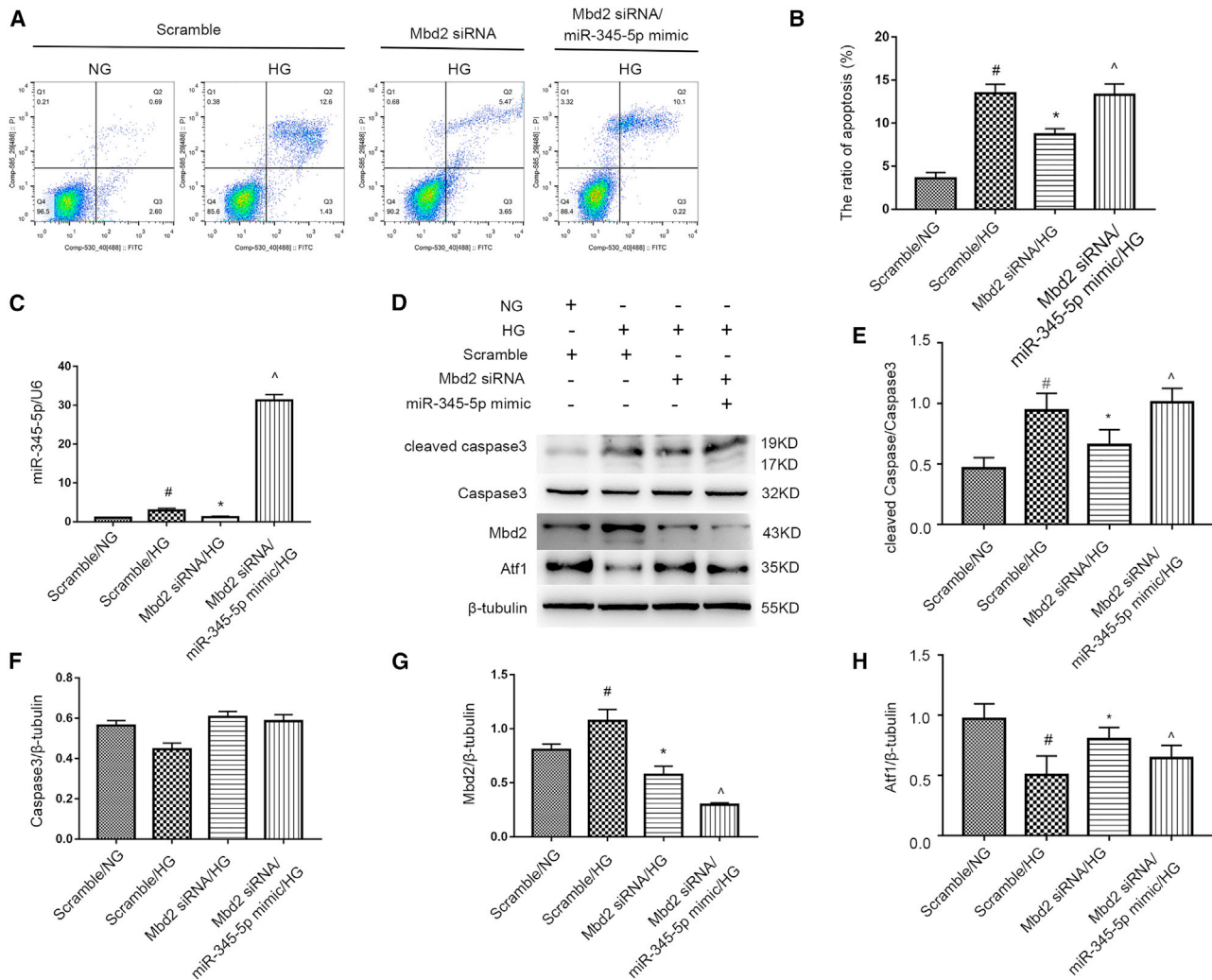


Figure 6. Mbd2 regulated apoptosis in RGCs by targeting miR-345-5p

(A and B) RGCs were co-transfected with 50 nM Mbd2 siRNA and miR-345-5p mimic following 72 h of HG interference. The rate of apoptosis was then analyzed by flow cytometry. (C) RT-qPCR was used to detect the expression of miR-345-5p. Expression changes in the protein levels of Mbd2, Atf1, and cleaved caspase3 after the transfection of Mbd2 siRNA and miR-345-5p mimic (D), and gray analysis of western blotting as normalized by β -tubulin and caspase3 (E–H).

Data are shown as the mean \pm SD of five independent experiments; #p < 0.05 versus Scramble/NG; *p < 0.05 versus Scramble/HG; ^p < 0.05 versus Mbd2 siRNA/HG.

the diabetic Mbd2^{+/+} retina (Figures 7A and 7B). Furthermore, the number of apoptotic cells in the ganglion cell layer induced by diabetes was lower in Mbd2^{-/-} mice than in the Mbd2^{+/+} mice (Figures 7C and 7D). Apart from morphological changes in the retina, another significant factor to consider is visual function. In order to analyze this aspect, we recorded electroretinography (ERG). The amplitudes of a-waves and b-waves in hyperglycemic mice were significantly lower when compared with mice from the control group; however, the impairment of visual function was alleviated in the Mbd2 knockout mice (Figures 7E–7G). The expression of miR-345-5p and apoptosis-related genes were also detected in the retina. In accordance with our *in vitro* results, the expression levels of miR-345-5p (Figure 7H) and cleaved caspase3 were lower in the Mbd2^{-/-}/STZ

mice than in the Mbd2^{+/+}/STZ mice (Figures 7I and 7J). These data suggested the deletion of Mbd2 in diabetic mice protects RGCs from apoptosis via the Mbd2/miR-345-5P/Atf1 pathway (Figure 8).

DISCUSSION

Previous studies suggested that DNA methylation is involved in the pathogenesis of diabetes and DR.^{9,10} Mbd2 is an interpreter of DNA methylation. Our recent work showed that Mbd2 mediates retinal cell apoptosis following ischemia/reperfusion injury.¹⁵ In the current study, we directly investigated the role of Mbd2 in the mechanisms underlying apoptosis in RGCs in both HG conditions and the diabetic retina. For the first time, we report that Mbd2 mediates HG-induced apoptosis in RGCs. *In vivo*, Mbd2 knockout mice notably

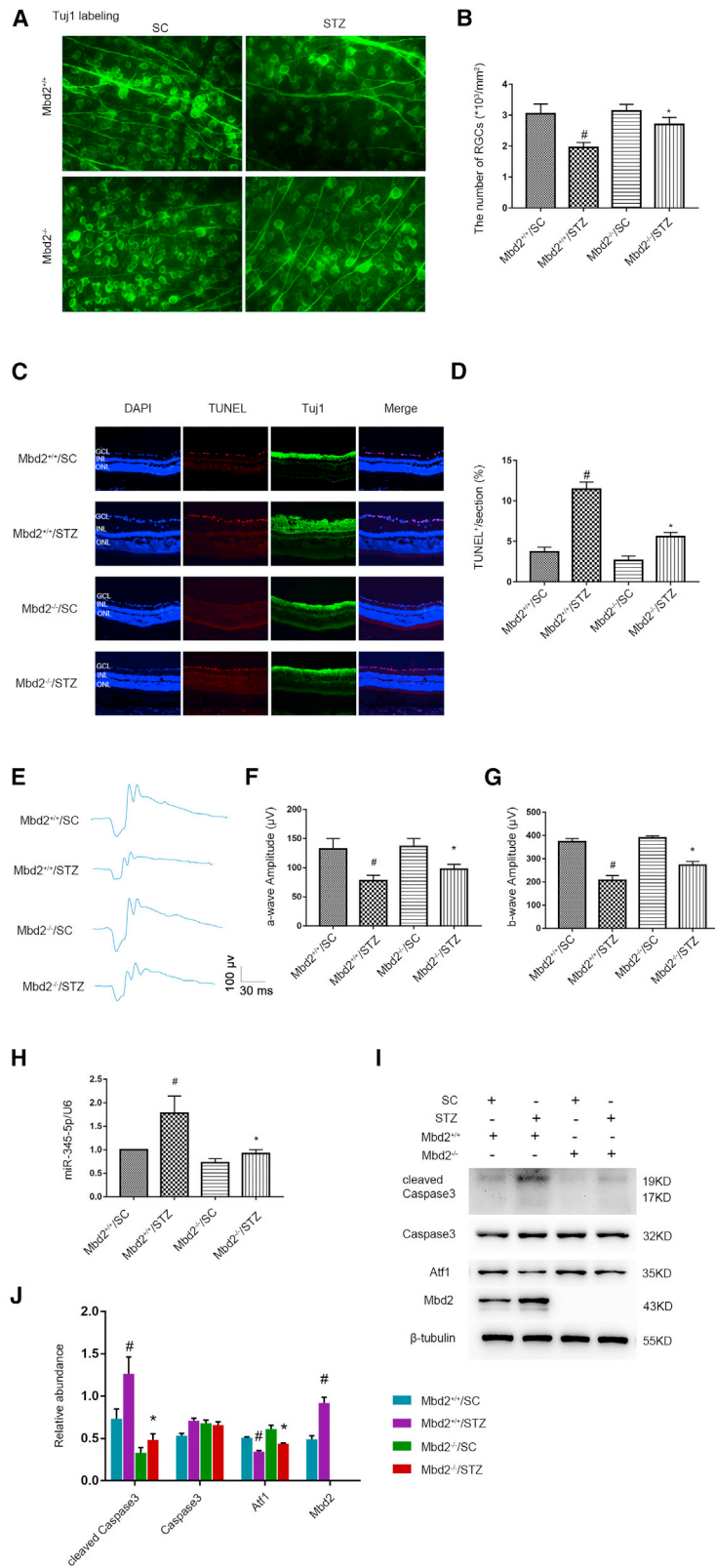


Figure 7. The apoptosis of RGCs in the diabetic retinas from Mbd2 knockout mice

Mice were anesthetized and the eyes and retinas were removed 12 weeks after STZ injection. Retina flat-mount and RGC immunofluorescence staining of Tuj1 (green) (A) and the number of surviving RGCs from mice with DR (B). Scale bar, 50 µm. Cryo-sections of retina sections were stained with TUNEL (red) (C) and the proportion (%) of cells undergoing apoptosis in the retina ganglion cell layer was analyzed (D). Scale bar, 100 µm. (E) ERG detection in the mice retina when stimulated by a flashing light with an intensity of 3.0 cd·s/m². Statistical analysis of a-wave amplitudes (F) and b-wave amplitudes (G). RT-qPCR detection of the expression of miR-345-5p in the retina (H). The expression of Mbd2, Atf1, and cleaved caspase3, at the protein level was detected by western blotting (I). Statistical analysis of western blotting as normalized by β-tubulin and caspase3 (J).

Data are shown as the mean ± SD of five independent experiments; #p < 0.05 versus Mbd2^{+/+}/SC; *p < 0.05 versus Mbd2^{+/+}/STZ.

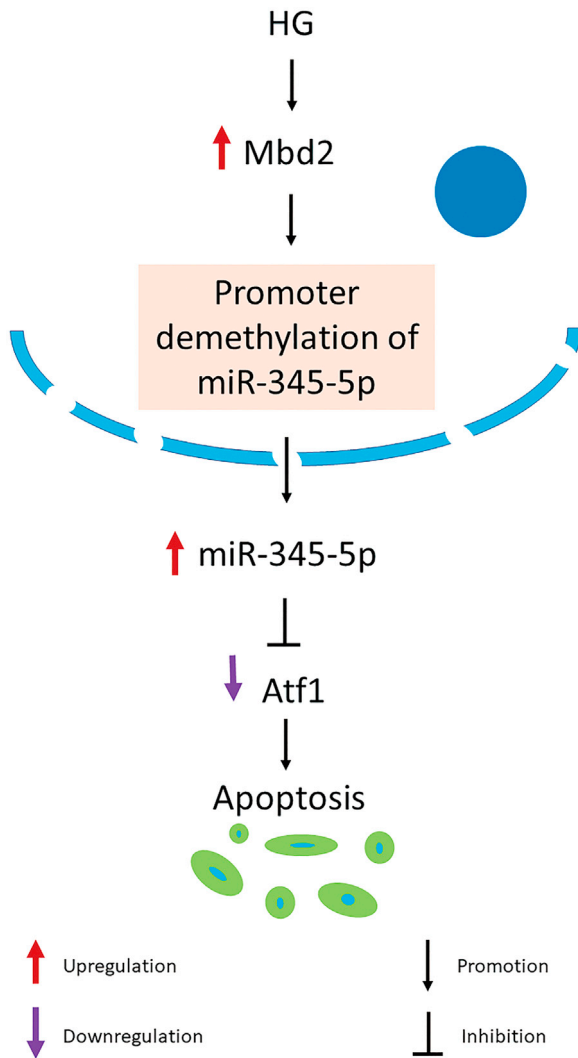


Figure 8. A schematic diagram showing the mechanism by which Mbd2 regulates HG-induced apoptosis in RGCs via the miR-345-5p/Atf1 axis
HG induced the expression of Mbd2, which then upregulates the expression of miR-345-5p. This suppresses the anti-apoptosis function of Atf1 via the demethylation of miR-345-5p.

attenuated the STZ-induced apoptosis of RGCs; this was accompanied by a partial improvement in visual function. Mechanistically, we found that Mbd2 directly upregulated the expression of miR-345-5p by suppressing promoter methylation, thus resulting in the apoptosis of retinal neural cells following exposure to HG.

First, we evaluated whether HG could induce the expression of Mbd2. Western blotting analysis revealed a significant increase in the expression levels of Mbd2 in primary RGCs at 24 h and 72 h following HG stimulation. As stated earlier, Mbd2 has been reported to be highly expressed in brain tissues²⁸ and induced in the rat hippocampus following cerebral ischemia.²⁹ *In vivo* immunofluorescence images also showed that the expression levels of Mbd2 increased in RGC

layers at 12 weeks after STZ-induced diabetes. Interestingly, this change was also observed in the inner and outer nuclear layers of the retina, implying that the function of Mbd2 in other retinal cells may need further investigation in the future. More recently, a study demonstrated that the loss of Mbd2 ameliorated the apoptosis of human kidney tubular epithelial cells in vancomycin-induced acute kidney injury.¹⁴ In our present study, we demonstrated that both Mbd2 siRNA *in vitro*, and Mbd2 knockout mice *in vivo*, can ameliorate apoptosis in RGCs under HG conditions. These data suggest that Mbd2 mediates the progression of apoptosis in retinal neuronal cells in diabetic retina, at least in part.

Next, we investigated the mechanisms associated with the action of Mbd2 in the pathogenesis of HG-induced retinal cell apoptosis. Interestingly, non-coding RNAs, particularly miRNAs, show broader associations with epigenetic regulation and many miRNAs are known to be regulated by epigenetic modifications, including DNA methylation.^{30,31} Mbd2 is a methylated-CpG binding protein. A recent study reported that miR-301a-5p was regulated by epigenetic mechanisms in vancomycin-induced acute kidney injury and that Mbd2 bound to the methylated-CpG within a region of the miR-301a-5p promoter, thus suppressing its methylation.¹⁴ We performed microarray analysis and confirmed that the expression levels of miR-345-5p were significantly increased in response to HG treatment, both *in vitro* and *in vivo*. In addition, ChIP assays showed that Mbd2 promoted the demethylation of miR-345-5p in its promoter region. The role of miRNAs in apoptosis has become a key focus for researchers seeking to gain a better understanding of the diabetic retina.³² We investigated the exact role of miR-345-5p in HG-related injury. Our results revealed that Mbd2 siRNA induced the downregulation of miR-345-5p and also alleviated the apoptosis of RGCs following HG injury. Interestingly, the overexpression of miR-345-5p could reverse this effect. Previously, miR-345-5p has been implicated in the proliferation of leukemia cells in acute myeloid leukemia.³³ MiR-345 has also been identified as a methylation-sensitive miRNA and its hyper-methylation can suppress the apoptosis of colon cancer cells.³⁴ In our present study, we verified the pro-apoptotic effects of miR-345-5p in RGCs under HG conditions, as shown by a reduction in the numbers of apoptotic cells and cleaved caspase3 following the administration of anti-miR-345-5p. These findings provide further evidence for the pro-apoptosis role of miR-345-5p in HG-induced retinal cell death.

We also investigated the target gene for miR-345-5p, which participates in the process of apoptosis. miRNAs are known to regulate gene expression post-transcriptionally by binding to the 3' UTR of target mRNA.^{35,36} Based on miRbase, data arising from previous studies,²⁷ we focused on Atf1, which activates genes, including BRAF, NRAS, MYC, BIRC2, DAAM1, MAML2, STAT1, ID1, and NKD2, related to apoptosis, Wnt, TGF- β , and MAPK pathways, and these effects cooperatively increase the risk of colorectal cancer.²⁵ Meanwhile, both RT-qPCR and immunoblot results showed that the expression of Atf1 was decreased under HG conditions at different time points *in vitro* and that the inhibition of miR-345-5p could

potentially reverse this trend. Deletion of the *Atf1* gene by siRNA significantly aggravated HG-induced apoptosis and increased the expression levels of cleaved caspase3 in RGCs, thus indicating that *Atf1* is an anti-apoptosis factor, as reported previously.^{25,37} These results highlighted that miR-345-5p targets the anti-apoptosis gene *Atf1* in the pathogenesis of retinal cell death following HG injury. Interestingly, the overexpression of miR-345-5p could partially reverse the reduced levels of HG-induced apoptosis in RGCs following the administration of *Mbd2* siRNA.

We also use knockout mice to investigate the function of *Mbd2* in the diabetic retina *in vivo*. We observed a significant increase in the number of RGCs in *Mbd2*^{-/-} mice that survived after 5 consecutive days of STZ injection when compared with those in *Mbd2*^{+/+} mice. In addition to a reduced level of cleaved caspase3 and the number of apoptotic cells, we also found that the expression levels of miR-345-5p were also reduced in the retinas of *Mbd2*^{-/-} mice when compared with *Mbd2*^{+/+} mice. These observations support the view that *Mbd2* mediates HG-related apoptosis in cells of the diabetic retina and that this occurs via a pathway in which miR-345-5p inhibits activation of the anti-apoptosis gene *Atf1*. The deletion of *Mbd2* in mice protected RGCs from diabetes-induced apoptosis in the retina. Collectively, our results indicate that *Mbd2* might represent a viable epigenetic target for the inhibition of retinal neurodegeneration in diabetes mellitus.

MATERIALS AND METHODS

Experimental animals

C57BL/6J mice were purchased from the Jackson Laboratory (Bar Harbor, ME), and *Mbd2* knockout mice were purchased from Cyagen Biosciences Co., Ltd (Guangzhou, China), as described previously.¹⁵ Male mice (6 to 8 weeks of age) were intraperitoneally injected with STZ (50 mg/kg) (V900890; Sigma-Aldrich, St. Louis, MO) dissolved in freshly prepared 0.1 M SC buffer (pH 7.4) for 5 consecutive days.^{38,39} After STZ injection, we measured blood glucose levels at random twice a week. All mice had free access to food and water. Only mice with a basal blood glucose level above 250 mg/dL were considered to be diabetic and used for further tests. Littermates that received SC injection served as controls. Animals were maintained in a room with 12-h light/dark cycles. Food and water were provided *ad libitum* and body weight was recorded fortnightly. All animal experiments were performed in accordance with a protocol approved by the Institution of Animal Care and Use Committee of the Second Xiangya Hospital and adhered to the Guidelines for the Care and Use of Laboratory Animals.

Isolation of primary RGCs

Primary RGCs were isolated from newborn mice (1 to 4 days old), as described previously.^{5,40} Retinas were dissected and washed in Dulbecco's PBS, and then placed in papain solution (0.6 mg/mL, G8430; Solarbio, Beijing, China) and DNase (125 U/mL, D4527; Sigma, St. Louis, MO) for dissociation at 37°C for 15 min. Retinal cells were then incubated in a solution containing 6 mL of ovomucoid containing 1.5 mg/mL of trypsin inhibitor (4,693,159,001; Roche, Basel, Switzerland). An antimacrophage antibody (AIA31240; Accurate

Chemical) was added to retinal cell suspensions. The cell suspensions were then incubated in flasks coated with donkey anti-rabbit immunoglobulin (Ig)G (H and L) (ab150075; Abcam, Cambridge, MA) at room temperature (RT) for 40 min. After filtration through a Nitex mesh (352,350; BD Biosciences, Franklin Lakes, NJ), the cells were transferred to a dish pre-coated with anti-Thy1.2 (M7898; Sigma) and pan for 1 h. Bound cells were released from the panning dish by the addition of 2.5% trypsin (T9201; Sigma). Finally, dissociated cells were plated on poly-d-lysine (P6407; Sigma)/laminin (L6274; Sigma)-coated 24-well plates, and subsequently cultured in neurobasal medium (1,103,049; Gibco, Grand Island, NY) supplemented with 10% penicillin-streptomycin, 50 ng/mL insulin (I6634; Sigma), 1 mM sodium pyruvate (51,300,044; Thermo Scientific, Waltham, MA), 1% L-glutamine (25,030,081; Thermo Scientific), 5 ng/mL N-acetyl cysteine (A8199; Sigma), 2% B27 (17,504,044; Thermo Scientific), 50 ng/mL brain-derived neurotrophic factor (248-BDB-050/CF; R&D Systems, Minneapolis, MN), 10 ng/mL ciliary neurotrophic factor (257-NT-010/CF; R&D Systems), 10 ng/mL forskolin (1099/10; R&D Systems), and 10 ng/mL basic fibroblast growth factor (3139-FB-025/CF; R&D Systems) in a humid incubator at 37°C supplied with 5% CO₂ and 95% O₂. Immunofluorescence staining of Tuj1 (1:500, GB11139; Servicebio, Wuhan, China) showed that the purity of RGCs was more than 95%.

The transfection of RGCs and HG interference

Lipofectamine 2000 was used for the transfection of plasmids and siRNA, including *Mbd2* siRNA, *Atf1* siRNA, miR-345-5p mimic and inhibitor, and *Mbd2* plasmid (Ribobio Co., Guangzhou, China) in Opti-MEM (31,985-070; Gibco) before HG or normal glucose (NG) treatment. In accordance with the manufacturer's instructions, when the density of the RGCs reached 80% to 90%, we added the pre-prepared 50-nM transfection solution to the cell culture dish. After 6 h, the transfection solution was removed and replaced with whole growth medium. To establish an *in vitro* model of HG damage, RGCs were exposed to a high concentration of D-glucose (33.3 mM) for 48 to 72 h.⁴¹ A negative control group was cultured with 5 mM glucose.

Flow cytometry

RGCs were trypsinized and washed gently with PBS, and then resuspended in 1 × Binding Buffer. Fluorescein isothiocyanate Annexin V (5 μL) and PI (5 μL) (556,457; BD Biosciences) were added to 100 μL of cell suspension (1 × 10⁶ cells/mL). Cells were subsequently incubated for 15 min at RT in the dark. Following incubation, we added 400 μL 1 × Binding Buffer. A FACSCalibur Cell Sorter (BD Biosciences) was used to detect cell apoptosis and data were analyzed by FlowJo V10 software.

Western blotting

Western blotting was performed as described previously.⁴² In brief, proteins were first extracted from cells or retinal tissues. Total protein (30 μg) was then loaded and separated on 10% SDS-PAGE gels and then transferred to polyvinylidene difluoride membranes. Blots were incubated with a primary antibody against *Mbd2* (ab188474; Abcam), *Atf1* (11946-1-AP; Proteintech, Rosemont, IL), caspase3/

cleaved caspase3 (#9662; CST, Danvers, MA), and β -tubulin (#10094-1-AP; Proteintech) at 4°C overnight. The following morning, membranes were washed and incubated with a species-specific horseradish peroxidase-conjugated secondary antibody, Goat Anti-Rabbit IgG (SA00001-2; Proteintech), at RT for 1 h. Positive binding was detected by an enhanced chemiluminescence kit (WBKLSO500; Millipore, Burlington, MA) and captured by a Tanon 5200 multi. Protein levels were normalized to β -tubulin and were compared with controls.

Chromatin immunoprecipitation

ChIP was carried out in accordance with the manufacturer's instructions (17-371RF; Millipore). First, the crosslink between protein and DNA was fixed by adding 37% formaldehyde to the culture medium. Cells were then collected and washed three times in cold PBS and then resuspended in SDS lysis buffer. Then, the cell lysates were sonicated to 200 to 1,000 base pair length crosslinked DNA. Next, 10 μ L supernatant was pre-cleaned with Protein G Agarose and centrifuged at $4000 \times g$ for 1 min; the supernatant was then kept at 4°C to act as an input. Next, we added an anti-Mbd2 antibody and natural mouse IgG and incubated overnight at 4°C with rotation to pull down the immunoprecipitate (IP). Then, we placed 60 μ L of Protein G Agarose into each IP and incubated at 4°C with rotation for 1 h in order to collect the antibody/antigen/DNA complex. Elution was performed by adding 100 μ L of Elution Buffer to each tube (including the input) containing the antibody/agarose complex; this was incubated for 15 min at RT. Afterward, the crosslinking of the eluted protein/DNA complex was reversed by adding 5 M NaCl and incubating at 65°C for 5 h. DNA was then isolated and purified by adding 1 mL of Binding Reagent A and collecting the flow-through with a spin filter. PCR was then carried out to detect the isolated DNA. Five pairs of primer sequences are described in the [supplemental information](#).

Luciferase reporter assay

We transferred the promoter region of miR-345-5p into a pCpGfree-basic-Lucia (pCpGI) reporter construct (pcpgf-basic; InvivoGen, San Diego, CA), which included the CG DNA methylation target sequences. This was co-transfected with the renilla plasmid in each group; each group was also transfected with plasmids containing Mbd2, mutant Mbd2 (mtMbd2; featuring a mutation in the DNA methylation region), or a control. Next, we detected luciferase activity in accordance with the instructions provided by the manufacturer of the Dual-Luciferase Reporter Assay System (E1910; Promega, Madison, WI) kit. After 48 h of transfection, cells were lysed by $1 \times$ passive lysis buffer and then collected into a tube. Next, we carefully transferred 20 μ L of cell lysate into a luminometer tube containing 100 μ L of Luciferase Assay Reagent II (LAR II); we were then able to detect fluorescence from the firefly luciferase. Next, we added 100 μ L of Stop & Glo Reagent so that we could assay fluorescence from renilla luciferase. In each group, we normalized firefly luciferase activity by that of renilla luciferase. We also constructed a WT and mutant (MUT) 3' UTR region into the pmirGLO dual-luciferase vector; these constructs were then co-transfected with an miR-345-5p mimic or scramble construct.

Real-time qPCR

Stem-loop real-time qPCR was performed to detect the level of mature miR-345-5p. Total RNA was extracted from RGCs with Trizol reagent (Invitrogen, Carlsbad, CA) in accordance with the manufacturer's instructions. RNA was purified using a genomic DNA Eraser kit and then reverse-transcribed with a Prime Script RT reagent kit (RR047A; TaKaRa, Dalian, Liaoning, China). SYBR Green was used to detect the levels of associated genes on a Step One Plus real-time PCR system (Bio-Rad, Hercules, CA). The levels of miR-345-5p and Atf1 were normalized by those for U6 and GAPDH, respectively. The primers used for miR-345-5p, U6, Atf1, and GAPDH are described in the [supplemental information](#).

Retina whole mounts and the quantification of RGCs

Mice were anesthetized and killed 12 weeks after the injection of STZ. The eyes from each animal were enucleated and fixed in FAS eye fixation buffer (G1109; Servicebio) for 1 h. The retina was dissected and fixed in FAS and then dehydrated in 30% source solution. Retinas were then permeabilized with 10% Triton X100 and blocked in 10% BSA/PBS solution at RT for 1 h. The retinas were then incubated at 4°C overnight with an anti- β -tubulin-III (Tuj1) antibody diluted to 1:500 (GB11139; Servicebio). The following morning, the retinas were incubated in the dark at RT for 2 h with a secondary Goat Anti-Rabbit IgG H&L antibody (ab150077, Alexa Fluor 488; Abcam). The retinas were then washed three times with PBS, and then flat-mounted on glass slides with Fluoroshield mounting medium containing DAPI (1b104139; Abcam) and a coverslip. Images of RGCs in retinal flat-mounts were photographed in two different regions at a distance of 1 and 2 mm to the disc of each quadrant of the retina using a LEICA DMI3000B microscope equipped with fluorescence illumination (Wetzlar, Germany); eight regions were captured per retina in order to analyze the mean number of surviving RGCs.

Terminal-deoxy-transferase-mediated dUTP nick end-labeling assay

Following acquisition of the retinas, we removed the anterior section of each eye, including the cornea, iris, lens, and vitreous body. The remaining posterior cup was then embedded in optimum cutting temperature compound and frozen at -80°C . A freezing microtome was then used to cut 10- μ m cryo-sections of the posterior eye cups. Next, we used the Terminal-Deoxy-Transferase-Mediated dUTP Nick End-Labeling (TUNEL) (1,684,795; Roche) to detect apoptotic cells in the retina, particularly in the ganglion cell layer. All cryo-sections were permeabilized and incubated with TUNEL solution (including 50 μ L Enzyme Solution [TdT] and 450 μ L Label Solution [fluorescein-dUTP]) at 37°C for 1 h, and then mounted. Four randomly selected fields were analyzed in each section in order to quantify the proportion (%) of TUNEL-positive cells; this was normalized by the total number of nuclei in the ganglion cell layer. For each animal, we analyzed three sections of the central retina.⁴²

Electroretinography

ERG was performed with a Roland Electrophysiological Instrument (Roland Consult, Munich, Germany), as described previously.¹⁵ In

brief, the mice were dark-adapted overnight and then anesthetized with pentobarbital sodium (65 mg/kg). Next, 0.4% oxybuprocaine hydrochloride and 1% tropicamide were used to induce anesthesia in the cornea and to dilate the pupil. ERG was elicited by flash stimuli with a Ganzfeld photostimulator at an intensity of 3.0 cd·s/m². The amplitude of the a- and b-waves were detected and then analyzed.

Statistical analysis

Statistical analysis was performed using the Student's t-test or by one-way ANOVA. Two-way ANOVA was used to evaluate the statistical significance of the differences between multiple treatment groups at different time points. Data are expressed as means ± SEM of five independent experiments. p values less than or equal to 0.05 were considered to be statistically significant.

SUPPLEMENTAL INFORMATION

Supplemental information can be found online at <https://doi.org/10.1016/j.omtn.2021.10.026>.

ACKNOWLEDGMENTS

This work was supported by the National Natural Science Foundation of China (81770951, 82171088) and the Natural Science Foundation of Hunan Province (2018JJ3742, 2021JJ30935). The authors express their gratitude to EditSprings (<https://www.editsprings.com/>) for the expert linguistic services provided.

AUTHOR CONTRIBUTIONS

H.L. designed the research; Y.G. and R.Z. performed the experiments; Y.F. collected the data and did the statistical analysis; J.L. purchased the reagents; Y.G. wrote the manuscript; and H.L. and R.Z. revised the manuscript.

DECLARATION OF INTERESTS

The authors declare no competing interests.

REFERENCES

- Antonetti, D.A., Klein, R., and Gardner, T.W. (2012). Diabetic retinopathy. *N. Engl. J. Med.* 366, 1227–1239.
- van Dijk, H.W., Verbraak, F.D., Kok, P.H., Garvin, M.K., Sonka, M., Lee, K., et al. (2010). Decreased retinal ganglion cell layer thickness in patients with type 1 diabetes. *Invest. Ophthalmol. Vis. Sci.* 51, 3660–3665.
- van Dijk, H.W., Verbraak, F.D., Kok, P.H., Stehouwer, M., Garvin, M.K., Sonka, M., et al. (2012). Early neurodegeneration in the retina of type 2 diabetic patients. *Invest. Ophthalmol. Vis. Sci.* 53, 2715–2719.
- Simo, R., Stitt, A.W., and Gardner, T.W. (2018). Neurodegeneration in diabetic retinopathy: does it really matter? *Diabetologia* 61 (9), 1902–1912.
- Barres, B.A., Silverstein, B.E., Corey, D.P., and Chun, L.L. (1988). Immunological, morphological, and electrophysiological variation among retinal ganglion cells purified by panning. *Neuron* 1 (9), 791–803.
- Sohn, E.H., van Dijk, H.W., Jiao, C., Kok, P.H., Jeong, W., Demirkaya, N., et al. (2016). Retinal neurodegeneration may precede microvascular changes characteristic of diabetic retinopathy in diabetes mellitus. *Proc. Natl. Acad. Sci. U S A* 113, E2655–E2664.
- Barber, A.J., Lieth, E., Khin, S.A., Antonetti, D.A., Buchanan, A.G., and Gardner, T.W. (1998). Neural apoptosis in the retina during experimental and human diabetes. Early onset and effect of insulin. *J. Clin. Invest.* 102 (4), 783–791.
- Portela, A., and Esteller, M. (2010). Epigenetic modifications and human disease. *Nat. Biotechnol.* 28 (10), 1057–1068.
- Duraisamy, A.J., Mishra, M., Kowluru, A., and Kowluru, R.A. (2018). Epigenetics and regulation of oxidative stress in diabetic retinopathy. *Invest. Ophthalmol. Vis. Sci.* 59, 4831–4840.
- Reddy, M.A., Zhang, E., and Natarajan, R. (2015). Epigenetic mechanisms in diabetic complications and metabolic memory. *Diabetologia* 58, 443–455.
- Corso-Diaz, X., Jaeger, C., Chaitankar, V., and Swaroop, A. (2018). Epigenetic control of gene regulation during development and disease: a view from the retina. *Prog. Retin. Eye Res.* 65, 1–27.
- Ginder, G.D., and Williams, D.C. (2018). Readers of DNA methylation, the MBD family as potential therapeutic targets. *Pharmacol. Ther.* 184, 98–111.
- Rao, X., Zhong, J., Zhang, S., Zhang, Y., Yu, Q., Yang, P., et al. (2011). Loss of methyl-CpG-binding domain protein 2 enhances endothelial angiogenesis and protects mice against hind-limb ischemic injury. *Circulation* 123, 2964–2974.
- Wang, J., Li, H., Qiu, S., Dong, Z., Xiang, X., and Zhang, D. (2017). MBD2 upregulates miR-301a-5p to induce kidney cell apoptosis during vancomycin-induced AKI. *Cell Death Dis.* 8, e3120.
- Ge, Y., Zhang, R., Feng, Y., and Li, H. (2020). Mbd2 mediates retinal cell apoptosis by targeting the lncRNA Mbd2-AL1/miR-188-3p/Traf3 Axis in ischemia/reperfusion injury. *Mol. Ther. Nucleic Acids* 19, 1250–1265.
- Slattery, M.L., Mullany, L.E., Sakoda, L.C., Wolff, R.K., Samowitz, W.S., and Herrick, J.S. (2018). Dysregulated genes and miRNAs in the apoptosis pathway in colorectal cancer patients. *Apoptosis* 23 (3–4), 237–250.
- Cheng, A.M., Byrom, M.W., Shelton, J., and Ford, L.P. (2005). Antisense inhibition of human miRNAs and indications for an involvement of miRNA in cell growth and apoptosis. *Nucleic Acids Res.* 33, 1290–1297.
- Su, W., Li, Z., Jia, Y., Zhu, Y., Cai, W., Wan, P., et al. (2017). microRNA-21a-5p/PDCD4 axis regulates mesenchymal stem cell-induced neuroprotection in acute glaucoma. *J. Mol. Cell. Biol.* 9, 289–301.
- Zhang, Q.L., Wang, W., Li, J., Tian, S.Y., and Zhang, T.Z. (2015). Decreased miR-187 induces retinal ganglion cell apoptosis through upregulating SMAD7 in glaucoma. *Biomed. Pharmacother* 75, 19–25.
- Kong, N., Lu, X., and Li, B. (2014). Downregulation of microRNA-100 protects apoptosis and promotes neuronal growth in retinal ganglion cells. *BMC Mol. Biol.* 15, 25.
- Shao, Y., Yu, Y., Zhou, Q., Li, C., Yang, L., and Pei, C.G. (2015). Inhibition of miR-134 protects against hydrogen peroxide-induced apoptosis in retinal ganglion cells. *J. Mol. Neurosci.* 56, 461–471.
- Yu, J., Zhang, B., Zhang, H., Qi, Y., Wang, Y., Wang, W., et al. (2019). E2F1-induced upregulation of long non-coding RNA LMCD1-AS1 facilitates cholangiocarcinoma cell progression by regulating miR-345-5p/COL6A3 pathway. *Biochem. Biophys. Res. Commun.* 512, 150–155.
- Tinay, I., Tan, M., Gui, B., Werner, L., Kibel, A.S., and Jia, L. (2018). Functional roles and potential clinical application of miRNA-345-5p in prostate cancer. *Prostate* 78, 927–937.
- Mou, T., Xie, F., Zhong, P., Hua, H., Lai, L., Yang, Q., et al. (2019). MiR-345-5p functions as a tumor suppressor in pancreatic cancer by directly targeting CCL8. *Biomed. Pharmacother.* 111, 891–900.
- Tian, J., Chang, J., Gong, J., Lou, J., Fu, M., Li, J., et al. (2019). Systematic functional interrogation of genes in GWAS loci identified ATF1 as a key driver in colorectal cancer modulated by a promoter-enhancer interaction. *Am. J. Hum. Genet.* 105, 29–47.
- Guo, Y., Sun, W., Gong, T., Chai, Y., Wang, J., Hui, B., et al. (2017). miR-30a radiosensitizes non-small cell lung cancer by targeting ATF1 that is involved in the phosphorylation of ATM. *Oncol. Rep.* 37, 1980–1988.
- Liang, X., Zhou, D., Wei, C., Luo, H., Liu, J., Fu, R., et al. (2012). MicroRNA-34c enhances murine male germ cell apoptosis through targeting ATF1. *PLoS One* 7, e33861.
- Fan, G., and Hutnick, L. (2005). Methyl-CpG binding proteins in the nervous system. *Cell Res.* 15, 255–261.

29. Jung, B.P., Zhang, G., Ho, W., Francis, J., and Eubanks, J.H. (2002). Transient fore-brain ischemia alters the mRNA expression of methyl DNA-binding factors in the adult rat hippocampus. *Neuroscience* 115 (2), 515–524.
30. Yao, Q., Chen, Y., and Zhou, X. (2019). The roles of microRNAs in epigenetic regulation. *Curr. Opin. Chem. Biol.* 51, 11–17.
31. Sankrityayan, H., Kulkarni, Y.A., and Gaikwad, A.B. (2019). Diabetic nephropathy: the regulatory interplay between epigenetics and microRNAs. *Pharmacol. Res.* 141, 574–585.
32. Chen, Q., Qiu, F., Zhou, K., Matlock, H.G., Takahashi, Y., Rajala, R.V., et al. (2017). Pathogenic role of microRNA-21 in diabetic retinopathy through downregulation of PPARalpha. *Diabetes* 66, 1671–1682.
33. Ying, X., Zhang, W., Fang, M., Zhang, W., Wang, C., and Han, L. (2018). miR-345-5p regulates proliferation, cell cycle, and apoptosis of acute myeloid leukemia cells by targeting AKT2. *J. Cell. Biochem.*
34. Tang, J.T., Wang, J.L., Du, W., Hong, J., Zhao, S.L., Wang, Y.C., et al. (2011). MicroRNA 345, a methylation-sensitive microRNA is involved in cell proliferation and invasion in human colorectal cancer. *Carcinogenesis* 32 (8), 1207–1215.
35. Lu, T.X., and Rothenberg, M.E. (2018). MicroRNA. *J. Allergy Clin. Immunol.* 141, 1202–1207.
36. Molasy, M., Walczak, A., Szaflik, J., Szaflik, J.P., and Majsterek, I. (2017). MicroRNAs in glaucoma and neurodegenerative diseases. *J. Hum. Genet.* 62, 105–112.
37. Persengiev, S.P., and Green, M.R. (2003). The role of ATF/CREB family members in cell growth, survival and apoptosis. *Apoptosis* 8, 225–228.
38. Qiu, A.W., Liu, Q.H., and Wang, J.L. (2017). Blocking IL-17a alleviates diabetic retinopathy in rodents. *Cell Physiol. Biochem.* 41 (3), 960–972.
39. Feit-Leichman, R.A., Kinouchi, R., Takeda, M., Fan, Z., Mohr, S., Kern, T.S., et al. (2005). Vascular damage in a mouse model of diabetic retinopathy: relation to neuronal and glial changes. *Invest. Ophthalmol. Vis. Sci.* 46, 4281–4287.
40. Jiao, J., Huang, X., Feit-Leithman, R.A., Neve, R.L., Snider, W., Dartt, D.A., et al. (2005). Bcl-2 enhances Ca(2+) signaling to support the intrinsic regenerative capacity of CNS axons. *EMBO J.* 24 (5), 1068–1078.
41. Liu, W.Y., Liou, S.S., Hong, T.Y., and Liu, I.M. (2017). Protective effects of hesperidin (citrus flavonone) on high glucose induced oxidative stress and apoptosis in a cellular model for diabetic retinopathy. *Nutrients* 9, 1312.
42. Kim, Y.H., Kim, Y.S., Kang, S.S., Cho, G.J., and Choi, W.S. (2010). Resveratrol inhibits neuronal apoptosis and elevated Ca2+/calmodulin-dependent protein kinase II activity in diabetic mouse retina [J]. *Diabetes* 59, 1825–1835.